metals

MDPI

Article

Wear and Corrosion Performance of Ti-6Al-4V Alloy Arc-Coated TiN/CrN Nano-Multilayer Film

Cheng-Hsun Hsu *, Chun-Yin Lin and Jian-Xun Chen

Department of Mechanical and Materials Engineering, Tatung University, Taipei City 104, Taiwan; rupert475@gmail.com (C.-Y.L.); andy86507@gmail.com (J.-X.C.)
* Correspondence: chhsu@gm.ttu.edu.tw

Abstract: The objective of this study was to investigate the effect of varying bias parameters (−50 V, −100 V, and −150 V) on the properties of TiN/CrN multilayer films deposited on Ti-6Al-4V alloy using the cathodic arc deposition (CAD) technique. The deposited films were characterized for their composition, structure, morphology, thickness, adhesion, and hardness. Wear and polarization tests were also conducted to determine the optimal bias condition for wear and corrosion resistance. The results showed that the TiN/CrN films possessed a nano-multilayered structure comprising TiN and CrN phases. The hard coating significantly increased the surface hardness of Ti-6Al-4V alloy up to three–five times. The coated specimens demonstrated superior wear resistance compared to the uncoated, with the −150 V specimen exhibiting the least wear rate. Furthermore, the −150 V specimen had the highest polarization impedance value, indicating the best corrosion resistance compared to the other bias conditions. In short, the use of CAD-coated TiN/CrN multilayer film enhanced the surface properties of Ti-6Al-4V alloy, with the best wear and corrosion resistance achieved at −150 V bias. These novel findings have significant implications for improving the performance and durability of Ti-6Al-4V alloy components in various industrial applications.

Keywords: Ti-6Al-4V; cathodic arc deposition; TiN/CrN nano-multilayer film; wear resistance; corrosion resistance

Citation: Hsu, C.-H.; Lin, C.-Y.; Chen, J.-X. Wear and Corrosion Performance of Ti-6Al-4V Alloy Arc-Coated TiN/CrN Nano-Multilayer Film. *Metals* **2023**, *13*, 907. https://doi.org/10.3390/met13050907

Academic Editor: Petros E. Tsakiridis

Received: 14 April 2023
Revised: 3 May 2023
Accepted: 6 May 2023
Published: 7 May 2023

1. Introduction

Titanium is a popular metal due to its excellent properties, such as good corrosion resistance, lightweight, ease of processing, good biocompatibility, and higher specific strength than steel. It can be further improved by the addition of other elements to form titanium alloys, making them suitable for various engineering applications [1,2]. For example, Ti-6Al-4V alloy is one of the most widely used titanium alloys in the aerospace, biomedical, and chemical industries [3,4]. However, it is important to note that Ti-6Al-4V alloy has a drawback of weak wear resistance, making it unsuitable for high-stress friction applications.

Surface modification is a widely adopted technology to enhance the wear and corrosion resistance of metals. To meet the need for surface modification, several researchers [5–13] have investigated the effect of various coatings on the properties of Ti-6Al-4V alloy. For instance, B. Rahmati et al. [5] employed sputtering to deposit TaO_2 films on the Ti-6Al-4V substrate, resulting in improved corrosion resistance and durability owing to the excellent coating adhesion. Cheng et al. [6] employed plasma electrolytic oxidation (PEO) to create a coating on the Ti-6Al-4V alloy, consisting of rutile and anatase materials, along with the silicon and phosphorus species. The increased wear resistance in dry sliding wear tests is presumed to be due to the diversity in the coating's composition and morphology. Kaseem et al. [12] applied a micro-arc oxide (MAO) coating on the Ti-6Al-4V alloy, leading to improved corrosion resistance through the enhanced electrochemical stability of the coating. Vella et al. [13] investigated the impact of dual treatment with the shot peening (SP)

and physical vapor deposition (PVD) coatings on the tribocorrosion behavior of Ti-6Al-4V alloy. The results showed that the dual-treated samples displayed excellent corrosion-wear resistance while unobtrusively enhancing the corrosion performance of the Ti-6Al-4V substrate. In summary, the various surface treatments mentioned above had diverse effects on enhancing the properties of the Ti-6Al-4V alloy.

Cathodic arc deposition (CAD) is a PVD technique that has been used to deposit ceramic hard films onto metallic surfaces, with most of these coatings exhibiting excellent wear and corrosion resistance properties. For example, the application of nitride films (such as TiN, CrN, ZrN, CrYN, and TiAlN) on various metallic materials using CAD has been demonstrated to significantly strengthen their wear and corrosion resistance [14–20]. In previous studies [21–24], a dual-coating design comprising an electroless nickel plating interlayer and a ceramic hard coating on ductile iron showed good corrosion resistance. This is because the electroless nickel interlayer effectively fills the graphite holes on the surface of ductile iron, resulting in increased adhesion of the ceramic hard film to the substrate and improved surface properties. Additionally, several studies have also explored the performance of various multilayer coatings, showing the positive effects of surface modification [25–29].

In this study, CAD technology was used to deposit a multilayered TiN/CrN film onto the Ti-6Al-4V alloy. The negative bias processing parameter was varied during the coating process, and subsequently, thin film analysis, wear tests, and polarization tests were conducted to investigate the effect of negative bias on coating properties, wear resistance, and corrosion resistance. This research aimed to identify the optimal process parameters and evaluate the potential of TiN/CrN nano-multilayer coatings in improving the surface properties of Ti-6Al-4V alloy.

2. Materials and Methods

The materials and methods utilized in the study are presented in the following subsections to provide a clear understanding of the various work details.

2.1. Material Preparation and CAD Treatment

In this study, the experimental material was the commercial Ti-6Al-4V alloy bars. The chemical composition of the alloy was analyzed using glow discharge optical spectroscopy (GDOS), and the result is shown in Table 1. These bars were machined into disc-shaped substrates with a diameter of 25 mm and a thickness of 6 mm. Prior to the CAD coating process, the specimens underwent mechanical grinding and polishing to achieve a surface roughness of 0.06 μm (Ra value), ultrasonic cleaning with alcohol, and then drying with warm air.

Table 1. Chemical composition of the Ti-6Al-4V alloy in the study (wt.%).

Al	V	Fe	O	C	N	Ti
6.20	4.11	0.23	0.15	0.07	0.05	Bal.

The CAD treatment involved the use of two targets, Ti pure-metal (99.99%) and Cr pure-metal (99.99%), and the specimens were placed face-to-face in a vacuum chamber and passed into N_2 reactive gas for the deposition of TiN/CrN multilayer films. The bias voltage of the substrate was varied, which was mainly set at −50 V, −100 V, and −150 V. To monitor the substrate temperature during the CAD coating process, a thermocouple was placed near the specimen's holder. Table 2 provides more information on the processing parameters used in the study.

Table 2. The processing parameters of the CAD in the study.

Parameter	Value
Ti cathode current (A)	60
Cr cathode current (A)	60
Working pressure (Pa)	2.67
Ar^+ bombardment (V/min)	−700/10
Substrate bias (V)	−50, −100, −150
Substrate temperature (°C)	240
Rotation rate (rpm)	4
Deposition time (min.)	50

2.2. Analysis of Coating Characterization

Several analytical techniques were adopted in the study to evaluate the characterization of coated specimens. The cross-sectional morphology and film layer thickness were observed using a field emission scanning electron microscope (FESEM, Hitachi SU-8000, Tokyo, Japan). The coating structure was identified using an X-ray diffractometer (XRD, MAC Science-M21X, Tokyo, Japan) by scanning the angular range of 20° to 100° with Cu-Kα radiation. The chemical composition of the films was determined by electron probe microanalysis (EPMA, JEOL JXA-8530F Pus, Tokyo, Japan) for the Cr, Ti, and N elements.

The surface roughness of the specimens was assessed using a surface roughness analyzer (Mitutoyo SV-400, Kanagawa, Japan). The adhesion strength quality (ASQ) [30] of the films was determined by Rockwell C indentation testing with a 150 kg load to evaluate the adhesion between film and substrate. Nanoindentation measurements were conducted using a nanoindenter (MTS XP system, Cary, NC, USA) with a diamond Berkovich tip to determine the hardness and Young's modulus values of the films. The load-displacement curves were analyzed using the Oliver and Pharr method [31] with a load of 4 mN, and the values obtained for each coating condition were averaged from 20 indentations. In addition, the surface hardness (HV) of the specimens was measured before and after coating using a micro-hardness tester to understand the coating effect on the surface hardness of Ti-6Al-4V alloys. Each specimen was tested five times with a testing load of 100 g to obtain the average value.

2.3. Wear Testing

The study utilized a ball-on-disc tribometer (CSM Instruments, Needham, MA, USA) to perform wear tests under the following conditions: (1) no lubricant; (2) circular track with a 30 mm diameter against a 6.0 mm diameter WC-6%Co ball; (3) wear speed of 0.17 m/s; (4) a normal load of 3 N; and (5) at room temperature and 65% relative humidity. The friction coefficient and total travel distance of 600 m were recorded during the tests. The specimen's weight was measured before and after the test using a precision electronic scale ($\times 10^{-4}$ g) to calculate the wear rate. The worn surface of the specimens after the wear testing was examined using FESEM.

2.4. Corrosion Testing

To evaluate the corrosion behavior of the specimens with/without coating, anodic potentiodynamic polarization tests were performed. The tests used a potentiostat/galvanostat apparatus (EG&G model 263A, Baltimore, MD, USA) with a corrosive medium of 3.5 wt.% NaCl solution to simulate the seawater environment. A standard saturated calomel electrode (SCE) was used as a reference, and platinum was used as a counter- or auxiliary electrode. The contact area of specimens was 1 cm^2, and the tests were carried out at ambient temperature. The electrode potential range was raised from −0.7 V to 0.3 V at a scanning rate of 1 mV/s. All polarization curves were plotted after 30 min of free immer-

sion of the specimens to stabilize the open circuit potential (OCP). The corrosion potential (Ecorr), corrosion current density (Icorr), and polarization resistance (Rp) were obtained for each specimen according to both the polarization curve and the Tafel extrapolation method [32]. The corrosion rate of the corroded specimens was calculated from Faraday's law presented in the related literature [33,34]. FESEM examination was also performed to observe the corroded surface appearances of the specimens. In addition, the EDS analyses were used to confirm the corrosion products on the specimen's surface.

3. Results and Discussion

3.1. Coating Composition and Structure

The EPMA analysis revealed the chemical composition of the coatings, and the bias effect on the elemental content is shown in Figure 1. As compared, an increase in bias value leads to an increase in Ti content and a decrease in Cr content in the films, while the N content remains relatively constant. This outcome suggests that TiN is more likely to produce nitrides compared to CrN. This is because titanium has a higher affinity for nitrogen compared to chromium. In other words, titanium readily reacts with nitrogen to form nitrides, while chromium is less reactive with nitrogen. Therefore, TiN coatings typically have a higher nitrogen content compared to CrN coatings. Moreover, this trend becomes more pronounced as the bias value increases. These findings have significant implications for the coating morphology and surface roughness.

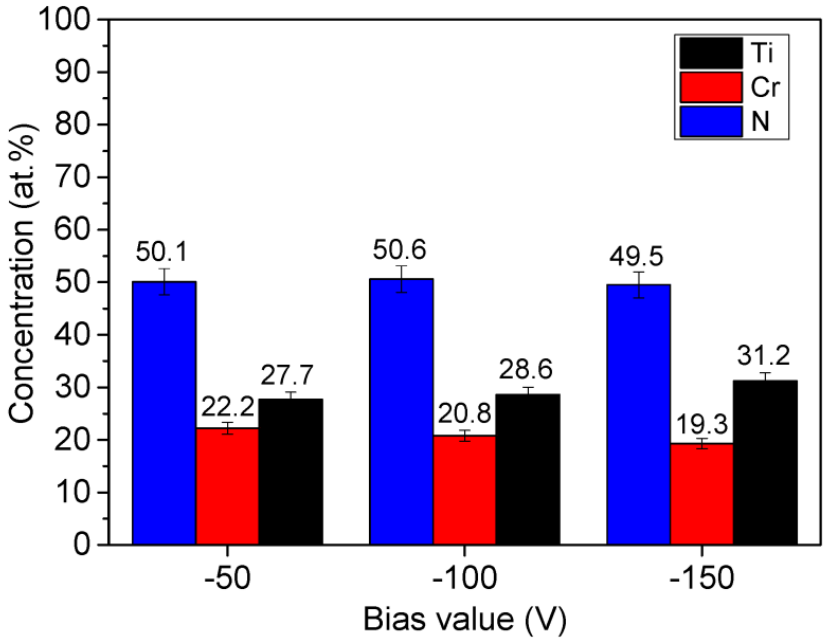

Figure 1. Bias effect on the elemental concentration of the films.

Figure 2 displays the XRD patterns of each coated specimen. The analysis indicates that the three films (−50 V, −100 V, −150 V) exhibit (111), (200), (220), (311), and (222) peaks, respectively, at the diffraction angle of 36.8°, 42.7°, 62.0°, 74.4°, and 78.3°, which are the overlapped peaks of TiN and CrN phases. Both TiN and CrN phases preferentially generate in the (111) plane, which is a specific crystal structure of sodium chloride type [35,36]. Therefore, the film structure mainly comprises TiN and CrN duplexes.

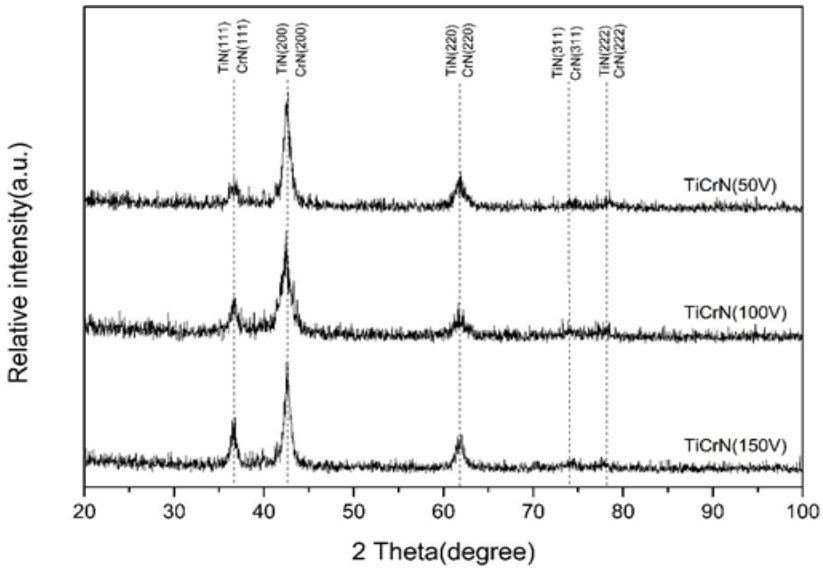

Figure 2. XRD patterns of the TiN/CrN films.

3.2. Coating Morphology and Thickness

The study utilized FESEM to observe the surface of Ti-6Al-4V substrates before and after coating, as depicted in Figure 3. The uncoated substrate had a polished state with a relatively flat surface, as shown in Figure 3a. After the coating treatment, a significant number of micro-droplets were deposited on the coated specimens, as illustrated in Figure 3b–d, where the −150 V specimen showed the least amount of micro-droplets. This is because, with an increase in the bias value, the film deposition rate decreases, resulting in a denser film layer and reducing the formation of micro-droplets. Therefore, the surface roughness tends to decrease as the bias value increases, which is confirmed by the comparison of Ra values among the specimens in Figure 4. The Ra values of the coated specimens in ascending order are −50 V, −100 V, and −150 V. Similarly, the film thickness tends to decrease as the bias value increases, as shown in Figure 5a–c. The order of film thickness is 5.71 μm for −50 V, followed by 4.13 μm for −100 V and 3.93 μm for −150 V. Thus, the bias value affects the deposition rate of the film; that is, as the bias value increases, the film thickness decreases, along with the surface roughness.

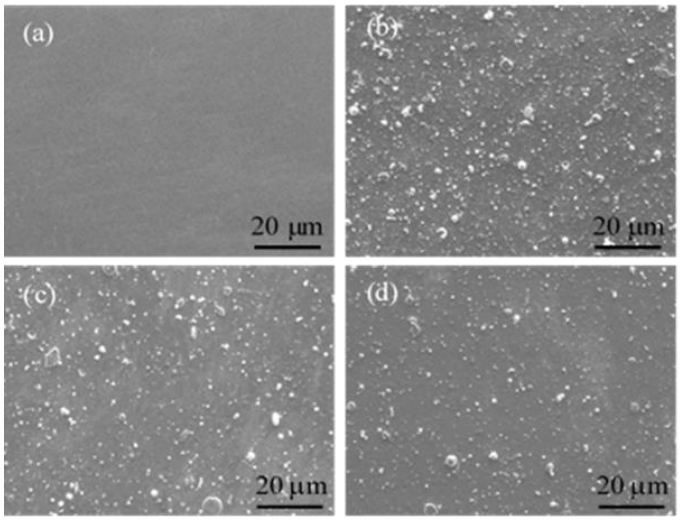

Figure 3. Surface appearance of the uncoated and coated specimens. (**a**) substrate, (**b**) −50 V, (**c**) −100 V, and (**d**) −150 V.

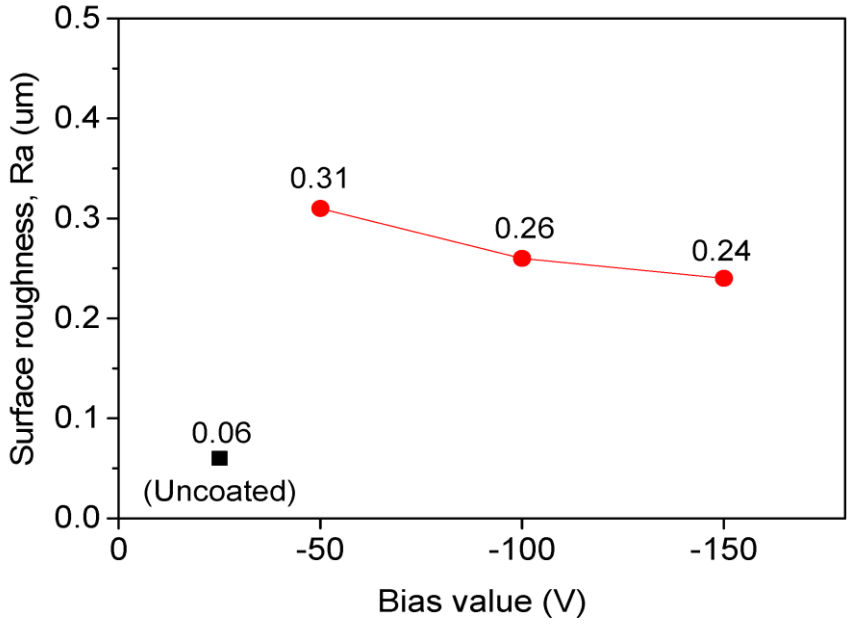

Figure 4. A comparison of surface roughness among the specimens.

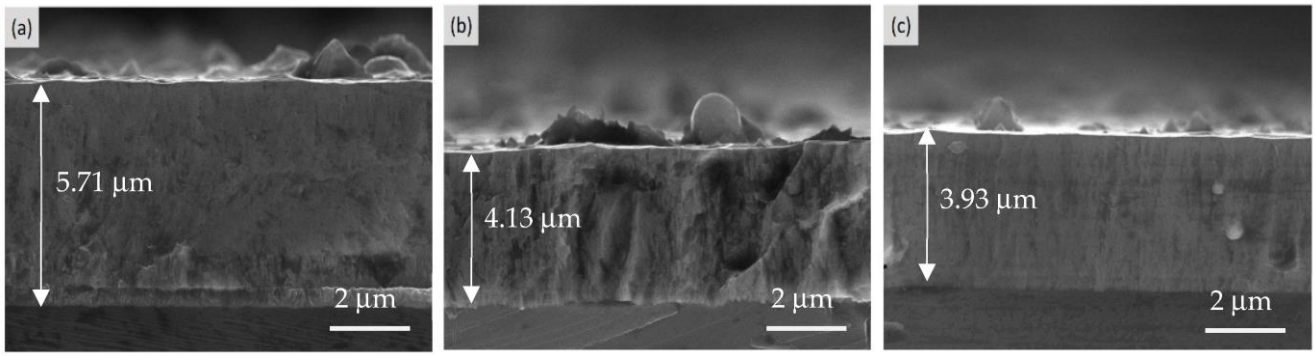

Figure 5. SEM cross-sectional view of the coated specimens. (**a**) −50 V; (**b**) −100 V; and (**c**) −150 V.

Figure 6 further provides a high-magnification scanning electron microscope (SEM) image to reveal a nano-multilayered structure of the film (−150 V). It can be observed that the duplexes in the multilayer have thicknesses of approximately 14.3 nm and 11.4 nm, respectively. Based on the relative amounts of titanium and chromium in the film, it is presumed that the thicker layer is titanium nitride (TiN), while the thinner layer is chromium nitride (CrN). In Figure 6, we can also see the typical structure of columnar crystals of CAD coating, as shown with the arrows. However, it is worth noting that the columnar structure of the film is not evident due to the multilayered formation, which impedes the growth of columnar crystals. Such a result may affect the corrosion behavior of Ti-6Al-4V coated with film, as discussed in Section 3.5.

3.3. Coating Adhesion and Hardness

The results of the adhesion test in the study are presented in Figure 7a–c, which shows the surface pattern of the coated specimens with different bias values after the indentation test. It is evident that there is no peeling observed around the indentation of the three coated specimens. Upon comparison with the ASQ standard [30], it can be observed that the three specimens display an indented appearance that falls close to HF1. This suggests that the adhesion of the TiN/CrN multilayered coating on Ti-6Al-4V is satisfactory and meets the required standards.

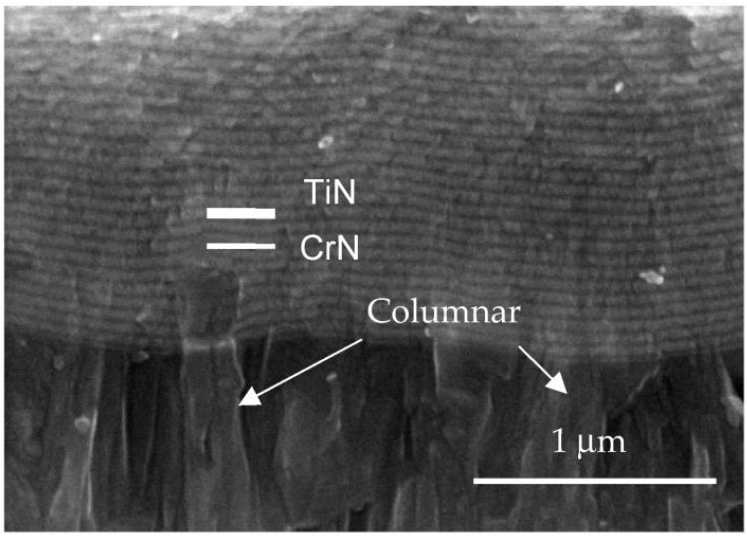

Figure 6. The SEM cross-sectional view of the nano-multilayered film.

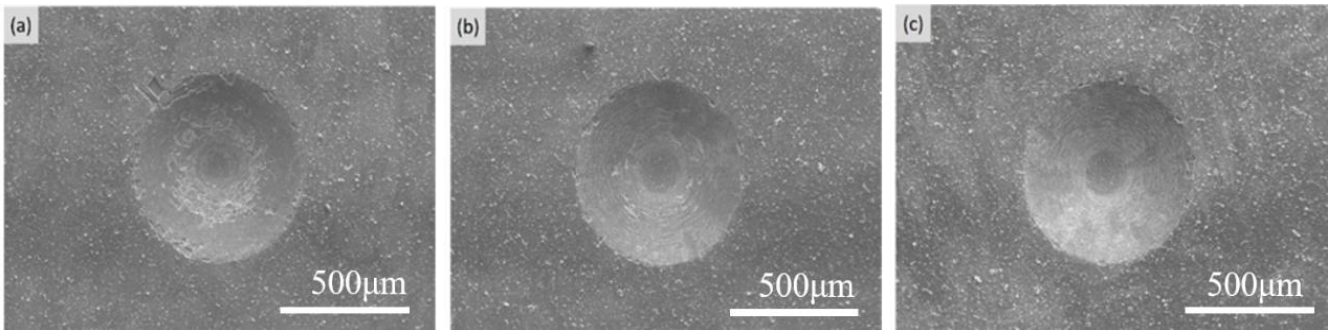

Figure 7. Fracture morphology of the coated specimens indented by Rockwell-C hardness tester. (**a**) −50 V; (**b**) −100 V; and (**c**) −150 V.

The nanoindentation hardness tests were performed to obtain the data containing film hardness (H), elastic modulus (E), and H/E value, as listed in Table 3. The data are compared in Figure 8a,b, and the results reveal a slight increase in film hardness with an increasing bias value. The −150 V specimen exhibits the highest hardness value (26.8 GPa) due to having the highest Ti content in the multilayer, which leads to the formation of more of the harder TiN phase. The elastic modulus of the three coatings ranges from 306.3 to 314.7 GPa, with an E value of 311.5 GPa for the −150 V specimen. Additionally, the values of H/E follow the order of −150 V > −100 V > −50 V. These findings may have an impact on the wear behavior of the film.

Table 3. Hardness (H); Elastic Modulus (E); and H/E values of the coated specimens.

Specimen	Hardness, H (GPa)	Elastic Modulus, E (GPa)	H/E
−50 V	24.0 ± 1.6	306.3 ± 12.4	0.078
−100 V	25.8 ± 1.3	314.7 ± 13.3	0.082
−150 V	26.8 ± 1.3	311.5 ± 13.8	0.086

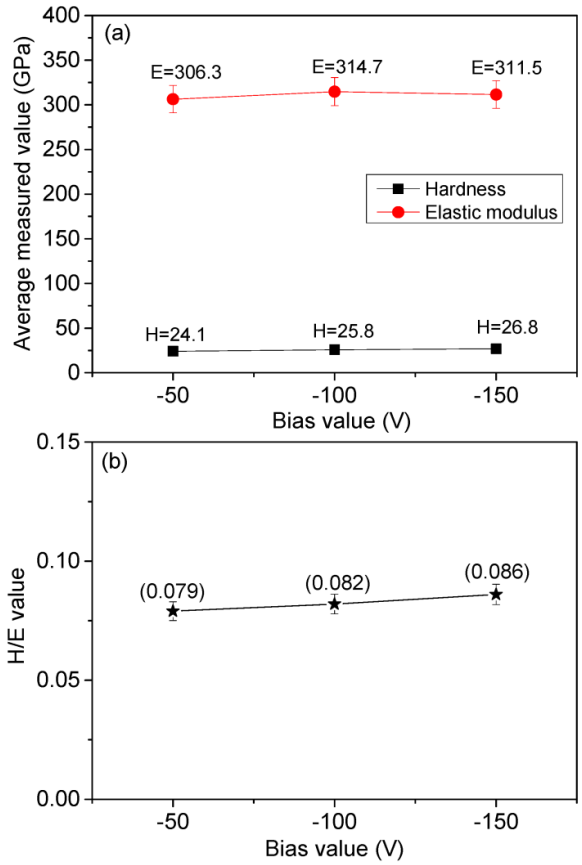

Figure 8. A comparison of (**a**) hardness, elastic modulus, and (**b**) H/E among the coatings.

On the other hand, the HV hardness test can mean to be a surface hardness index with a substrate effect for coated specimens, as the indentation depth of the HV hardness test is greater than the thickness of the film. In this study, a comparison of the HV hardness values among the specimens is shown in Figure 9. The result was similar to the nanoindentation hardness; it showed that Ti-6Al-4V has a significant increase in surface hardness from 333 HV to 1087–1765 HV after coating. The surface hardness of the coated specimen was promoted approximately three–five times more than the substrate. Furthermore, the hardness value of the coated specimen increased with increasing bias value, where the −150 V specimen had the highest surface hardness value (1765 HV).

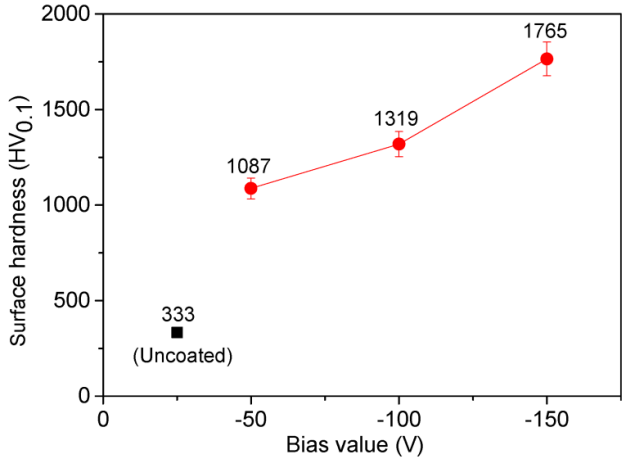

Figure 9. A comparison of surface hardness among the uncoated and coated specimens.

3.4. Analysis of Wear Behavior

Figure 10 compares the friction coefficients obtained for each specimen after the wear test. The result illustrates that the coated specimens have a higher friction coefficient compared to the Ti-6Al-4V specimen (0.6–0.8 vs. 0.4). This can be attributed to the fact that the uncoated specimen with the lowest roughness after grinding and polishing has a lower friction coefficient. A comparison of the coated specimens also shows that the friction coefficient tends to be the same as the surface roughness (see Figure 4). That is, the smaller the surface roughness, the lower the coefficient of friction. The friction coefficient of the specimen is thus directly dependent upon the surface roughness. In addition, another important indicator of wear test results is to use the wear rate to evaluate the wear resistance [37]. In this study, it was observed that the wear rate of the coated specimens was significantly lower than that of the uncoated ones, as illustrated in Figure 11. This suggests that TiN/CrN multilayered film-coated Ti-6Al-4V specimens can greatly enhance wear resistance. The wear rate of the coated specimens also correlates with the H/E value, which is in agreement with the literature [38]. Specifically, the higher the H/E value, the lower the wear rate, resulting in better wear resistance. Therefore, among the three coated specimens, the one with a potential of −150 V exhibited the lowest wear rate and, thus, displayed the best wear resistance.

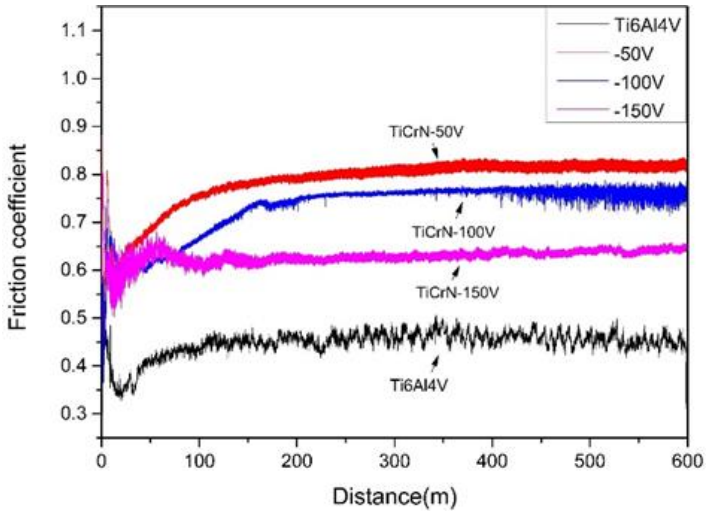

Figure 10. Comparison of friction coefficient among the specimens after wear tests.

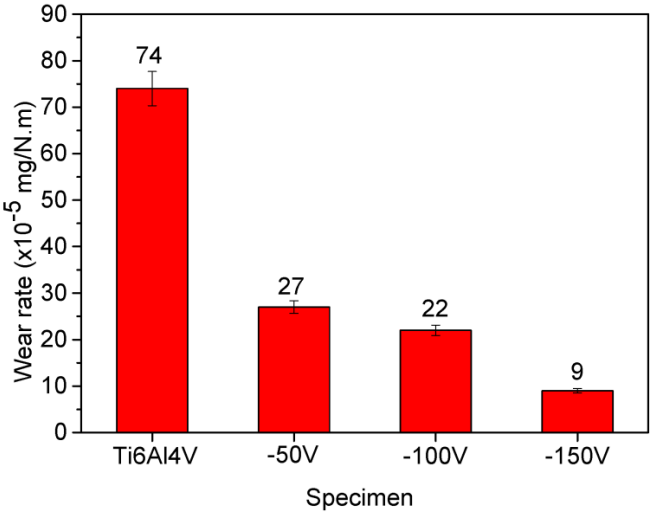

Figure 11. Comparison of wear rate among the specimens after wear tests.

Figure 12 is the surface image of each specimen after the wear testing, which further supports the results of the above wear tests. Figure 12a shows that the uncoated specimen had an adhesive wear mechanism with a deeper and wider worn track due to its low surface hardness. On the other hand, the coated specimens exhibited significantly higher hardness, leading to a lower wear rate and shallower wear marks as a result of the abrasive wear mechanism. This is illustrated in Figure 12b–d. It is clearly seen that the −150 V coated specimen had the highest hardness and, therefore, corresponded to the narrowest wear trajectory, as shown by the red dashed line in Figure 12d.

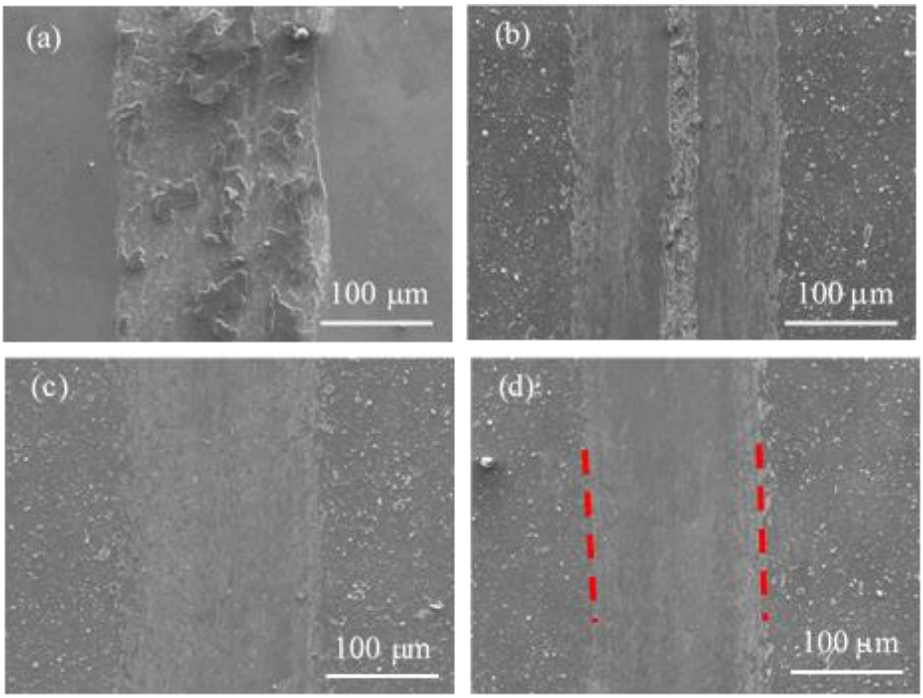

Figure 12. SEM photographs of the worn surface of the specimens after wear tests. (**a**) Ti-6Al-4V; (**b**) −50 V; (**c**) −100 V; and (**d**) −150 V (Red dotted line: the width of the wear track).

3.5. Analysis of Corrosion Behavior

Figure 13 displays the polarization curves of the specimens obtained from polarization tests. The data of corrosion potential (Ecorr), corrosion current density (Icorr), and polarization resistance (Rp) were determined from the curves to evaluate the corrosion resistance of each specimen, as presented in Table 4. The results revealed that the −150 V specimen had the highest corrosion potential and polarization resistance, indicating the best corrosion resistance among all specimens. However, the corrosion resistance of the coatings tends to decrease as the bias value decreases. This is likely due to the influence of micro-droplets and film density on the specimen's surface. The previous study also suggested that film density could be refined by higher negative bias [39]. In this study, the decrease in negative bias resulted in an increase in micro-droplets and holes to decay the corrosion resistance. In Figure 13, it is noted that there are current peaks in the anodic branch of polarization curves for the coated specimens. The appearance of current peaks in the anodic branch of polarization curves during a polarization test can be generally attributed to various phenomena, depending on the specific system being studied. In this study, one possible cause is the occurrence of localized corrosion, such as pitting corrosion, which can lead to the formation of preferential anodic sites on the surface. These sites can result in the formation of local anodic peaks in the polarization curve as the potential is increased. Such a result can be evidenced by the observation in Figure 14.

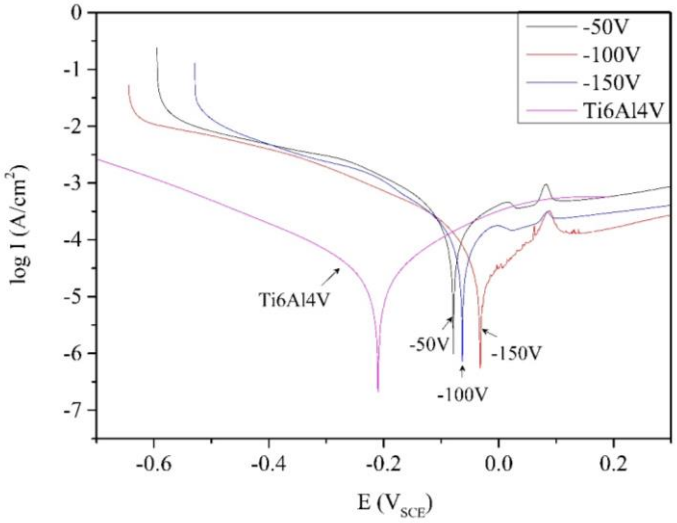

Figure 13. Polarization curves of the specimens obtained from polarization tests.

Table 4. Polarization data of the specimens after polarization tests.

Specimen	Ecorr. (V)	Icorr. ($\times 10^{-8}$ A/cm^2)	Rp (Ohm/cm^2)
Ti-6Al-4V	−0.21	2.6	337,595
−50 V	−0.09	7.1	208,718
−100 V	−0.08	6.5	348,665
−150 V	−0.06	5.8	412,951

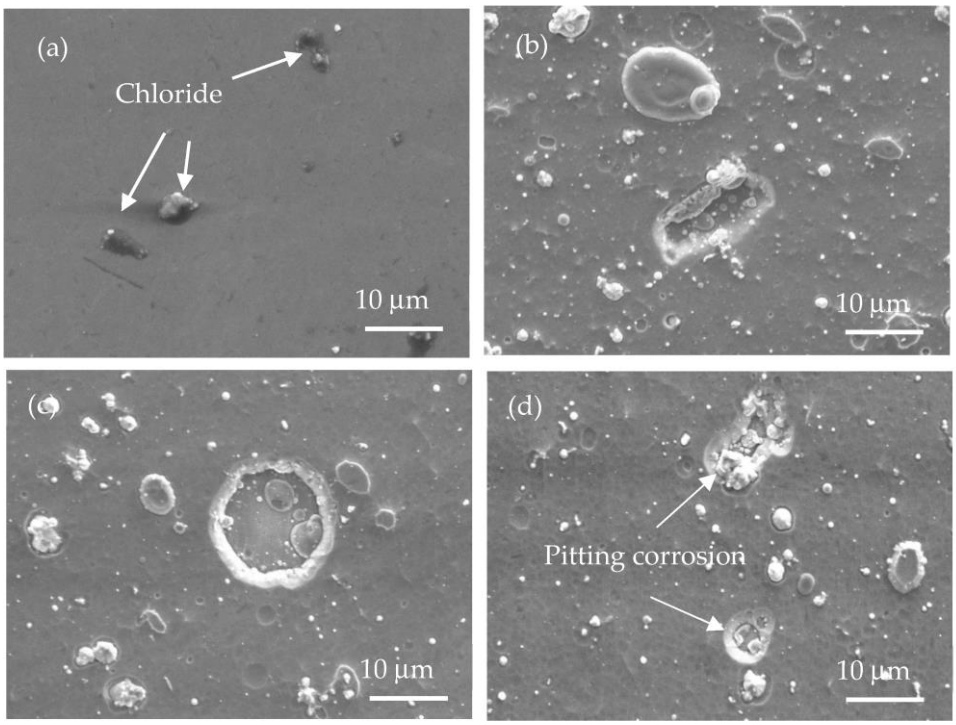

Figure 14. Surface morphology of the specimens after polarization tests in 3.5 wt.% NaCl solution: (**a**) Ti-6Al-4V; (**b**) −50 V; (**c**) −100 V; and (**d**) −150 V.

Figure 14 presents the surface appearance of each specimen after the corrosion test. The uncoated Ti-6Al-4V alloy seems to exhibit slight corrosion with only a trace amount of

chloride ($TiCl_4$) products because of its inherent resistance to saltwater corrosion (Figure 14a. As is known, this is inherently characterized by the formation of a dense TiO_2 layer on the surface of the Ti-6Al-4V alloy. Regarding the coated specimens shown in Figure 14b–d, the main corrosion behavior observed was the occurrence of pitting corrosion at the coating micro-droplets, as stated previously, with the −150 V specimen experiencing the least amount of pitting, as depicted in Figure 14d. This can be attributed to the fact that the −150 V specimen has the fewest micro-droplets on its surface, resulting in the best corrosion resistance. Additionally, it can be inferred that the multilayer structure acts as a barrier that prevents the corrosive medium from directly penetrating the substrate through the columnar grain boundaries.

Additionally, some literature suggested that the corrosion rate can be calculated using the corrosion current density obtained from the polarization curves [33,34]. In this study, the corrosion rate of the specimens was determined according to the relevant literature, and the results are presented in Figure 15. Comparing the corrosion rate data indicates that the coated specimens have a slower corrosion rate (0.46–0.57 × 10^{-4} mm/yr) than the uncoated ones (2.51 × 10^{-4} mm/yr), confirming that Ti-6Al-4V coated with TiN/CrN nano-multilayers can enhance corrosion resistance. Among all the specimens, the specimen coated at −150 V exhibits the lowest corrosion rate (0.46 × 10^{-4} mm/yr) to indicate the best corrosion resistance.

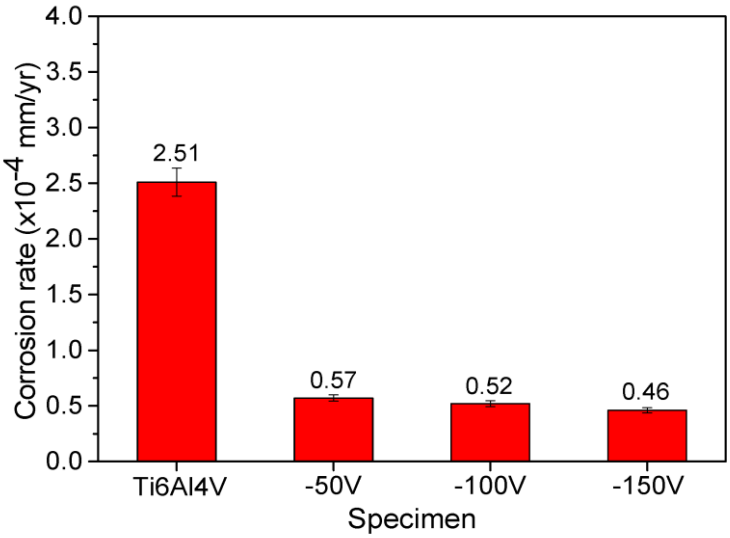

Figure 15. A comparison of corrosion rate of the uncoated and coated specimens.

4. Conclusions

1. The coating structure studied was primarily a nano-multilayered film, which was made up of alternating layers of TiN and CrN duplexes. The multilayer film demonstrated good adhesion to the Ti-6Al-4V substrate. As the bias value increased, the film thickness was thinner, but the film structure became denser, and the surface roughness was reduced.
2. The nanoindentation hardness and microhardness of the film increased as the bias value was raised, indicating a denser film structure. The specimen treated with a bias value of −150 V displayed the highest film hardness (26.8 GPa) and surface microhardness (1765 HV) among all the specimens.
3. The coated specimens exhibited a higher friction coefficient in comparison to the uncoated Ti-6Al-4V, which was due to the coating's increased surface roughness. However, despite this, the wear rate of the coated specimens was notably lower than that of the uncoated ones, indicating an improvement in abrasion resistance.
4. The Ti-6Al-4V alloy is well-known for its inherent ability to resist corrosion in saltwater environments. However, when coated with a TiN/CrN nano-multilayer film, it was

found that the specimen treated at bias values of −150 V demonstrated the highest corrosion potential and polarization resistance values, indicating an enhancement in corrosion resistance. Nevertheless, the coating effect on the corrosion resistance of the Ti-6Al-4V alloy is somewhat limited compared to the significant improvement observed in its wear resistance.

Author Contributions: Conceptualization, C.-H.H.; methodology, C.-H.H.; formal analysis, C.-H.H. and C.-Y.L.; data curation, C.-Y.L. and J.-X.C.; funding acquisition, C.-H.H.; investigation, C.-Y.L. and J.-X.C.; writing—original draft, C.-H.H.; Writing—review and editing, C.-H.H. All authors have read and agreed to the published version of the manuscript.

Funding: This research was funded by the National Science and Technology Council (MOST 111-2221-E-036-008) and Tatung University (B110-T01-027) in Taiwan.

Data Availability Statement: The data presented in this study can be available upon request from the corresponding author.

Acknowledgments: The authors would like to thank the National Science and Technology Council (MOST 111-2221-E-036-008) and Tatung University (B110-T01-027) in Taiwan (ROC) for the funding support.

Conflicts of Interest: The authors declare no conflict of interest.

References

1. Smith, W.F. *Materials Science and Engineering*; McGraw-Hill, Inc.: New York, NY, USA, 1993; p. 500.
2. Mangonon, P.L. *The Principles of Materials Selection for Engineering Design*; Prentice-Hall, Inc.: London, UK, 1999; p. 563.
3. Sha, W.; Malinov, S. Titanium Alloys. 2009. Available online: https://www.elsevier.com/books/titanium-alloys/sha/978-1-84569-375-6 (accessed on 1 January 2023).
4. Flinn, R.A.; Trojan, P.K. *Engineering Materials and Their Applications*; Houghton Mifflin Co.: Boston, MA, USA, 1990; p. 353.
5. Rahmati, B.; Sarhan, A.A.D.; Basirun, W.J.; Abas, W.A.B.W. Ceramic tantalum oxide thin film coating to enhance the corrosion and wear characteristics of Ti–6Al–4V alloy. *J. Alloys Compd.* **2016**, *676*, 369–376. [CrossRef]
6. Cheng, Y.L.; Wu, X.Q.; Xue, Z.G.; Matykina, E.; Skeldon, P.; Thompson, G.E. Microstructure, corrosion and wear performance of plasma electrolytic oxidation coatings formed on Ti–6Al–4V alloy in silicate-hexametaphosphate electrolyte. *Surf. Coat. Technol.* **2013**, *217*, 129–139. [CrossRef]
7. Farid, M.A.; Amir, A.; Mahmood, A.; Abedi, M. Improving the wear and corrosion resistance of Ti–6Al–4V alloy by deposition of TiSiN nanocomposite coating with pulsed-DC PACVD. *Wear* **2017**, *390–391*, 93–103.
8. Lee, C.K. Wear and corrosion behavior of electrodeposited nickel–carbon nanotube composite coatings on Ti–6Al–4V alloy in Hanks' solution. *Tribol. Inter.* **2012**, *55*, 7–14.
9. Pat, S.; Çakir, F.H.; Öteyaka, M. Corrosion behavior of graphene coated Ti-6Al-4V alloy by anodic plasma coating method. *Inorg. Chem. Commun.* **2023**, *147*, 110268. [CrossRef]
10. Narayanan, T.S.N.S.; Kim, J.; Hyung, W.P. High performance corrosion and wear resistant Ti-6Al-4V alloy by the hybrid treatment method. *Appl. Surf. Sci.* **2020**, *504*, 144388. [CrossRef]
11. Li, W.; Gao, J.; Ma, Y.; Zheng, K.; Zhi, J.; Xin, Y.; Xie, S.; Yu, S. Undoped and diamond-doped MAO coatings prepared on Ti6Al4V: Microstructure, wear, corrosion, and biocompatibility properties. *Surf. Coat. Technol.* **2023**, *458*, 129340. [CrossRef]
12. Kaseem, M.; Choe, H.C. The effect of in-situ reactive incorporation of MoOx on the corrosion behavior of Ti-6Al-4 V alloy coated via micro-arc oxidation coating. *Corros. Sci.* **2021**, *192*, 109764. [CrossRef]
13. Vella, K.A.; Buhagiar, J.; Cassar, G.; Pizzuto, M.M.; Bonnici, L.; Chen, J.; Zhang, X.; Huang, Z.; Zammit, A. The Effect of a Duplex Surface Treatment on the Corrosion and Tribocorrosion Characteristics of Additively Manufactured Ti-6Al-4V. *Materials* **2023**, *16*, 2098. [CrossRef]
14. Li, M.; Yu, Y.; Zou, C.; Tian, C.; Wang, Z.; Xiang, Y. Wear and corrosion resistance of CrYN coating in artificial seawater. *Metals* **2023**, *13*, 183. [CrossRef]
15. Kowalski, M.; Stachowiak, A. Tribocorrosion performance of Cr/CrN hybrid layer as a coating for machine components used in a chloride ions environment. *Coatings* **2021**, *11*, 242. [CrossRef]
16. Babur, M.Z.; Iqbal, Z.; Shafiq, M.; Naz, M.Y.; Makhlouf, M.M. Hybrid TiN-CCPN coating of AISI-201 stainless steel by physical vapor deposition combined with cathodic cage plasma nitriding for improved tribological properties. *J. Build. Eng.* **2022**, *45*, 103512. [CrossRef]
17. Supakanya, K.; Saikaew, C.; Anurat, W.; Surasak, S. Wear behaviours of filtered cathodic arc deposited TiN, TiAlSiN and TiCrAlSiN coatings on AISI 316 stainless steel fishing net-weaving machine components under dry soft-sliding against nylon fibres. *Wear* **2017**, *390−391*, 146–154.
18. Lin, M.T.; Wan, C.H.; Wu, W. Characterization and corrosion resistance of TiZr coating on SS304 stainless steel using cathodic arc evaporation techniques. *Surf. Coat. Technol.* **2017**, *320*, 217–225. [CrossRef]

19. Warcholinski, B.; Gilewicz, A.; Myslinski, P.; Dobruchowska, E.; Murzynski, D.; Kuznetsova, T.A. Effect of silicon concentration on the properties of Al-Cr-Si-N coatings deposited using cathodic arc evaporation. *Materials* **2020**, *13*, 4717. [CrossRef]
20. Xiang, Y.; Zou, C. Effect of arc currents on the mechanical, high temperature oxidation and corrosion properties of CrSiN nanocomposite coatings. *Coatings* **2022**, *12*, 40. [CrossRef]
21. Lin, C.K.; Hsu, C.H.; Cheng, Y.H.; Ou, K.L.; Lee, S.L. A study on the corrosion and erosion behavior of electroless nickel and TiAlN/ZrN duplex coatings on ductile iron. *Appl. Surf. Sci.* **2015**, *324*, 13–19. [CrossRef]
22. Hsu, C.H.; Huang, K.H.; Chen, Y.T.; Ho, W.Y. The effect of electroless Ni-P interlayer on corrosion behavior of TiN-coated austempered ductile iron. *Thin Solid Film.* **2013**, *529*, 34–38. [CrossRef]
23. Hsu, C.H.; Chen, K.L.; Lu, K.C. Effects of low-temperature duplex coatings on abrasive and erosive behavior of ADI. *Thin Solid Film.* **2011**, *519*, 4855–4859. [CrossRef]
24. Hsu, C.H.; Lee, C.Y.; Chen, K.L.; Lu, J.H. Effects of CrN/EN and Cr_2O_3/EN duplex coatings on corrosion resistance of ADI. *Thin Solid Film.* **2009**, *517*, 5248–5252. [CrossRef]
25. Rajabi, T.; Atapour, M.; Elmkhah, H.; Nahvi, S.M. Nanometric CrN/CrAlN and CrN/ZrN multilayer physical vapor deposited coatings on 316L stainless steel as bipolar plate for proton exchange membrane fuel cells. *Thin Solid Film.* **2022**, *753*, 139288. [CrossRef]
26. Jasempoor, F.; Elmkhah, H.; Imantalab, O.; Arash, F. Improving the mechanical, tribological, and electrochemical behavior of AISI 304 stainless steel by applying CrN single layer and Cr/CrN multilayer coatings. *Wear* **2022**, *504–505*, 204425. [CrossRef]
27. Pogrebnjak, A.; Smyrnova, K.; Bondar, O. Nanocomposite multilayer binary nitride coatings based on transition and refractory metals: Structure and properties. *Coatings* **2019**, *9*, 155. [CrossRef]
28. Frank, F.; Kainz, C.; Tkadletz, M.; Czettl, C.; Pohler, M.; Schalk, N. Microstructural and micro-mechanical investigation of cathodic arc evaporated ZrN/TiN multilayer coatings with varying bilayer thickness. *Surf. Coat. Technol.* **2022**, *432*, 128070. [CrossRef]
29. Vengesa, Y.; Arash, F.; Elmkhah, H.; Imantalab, O. Influence of post-deposition annealing temperature on morphological, mechanical and electrochemical properties of CrN/CrAlN multilayer coating deposited by cathodic arc evaporation-physical vapor deposition process. *Surf. Coat. Technol.* **2022**, *432*, 128090. [CrossRef]
30. Vidakis, N.; Antoniadis, A.; Bilalis, N. The VDI 3198 Indentation Test Evaluation of a Reliable Qualitative Control for Layered Compounds. *J. Mater. Proc. Technol.* **2003**, *143–144*, 481–485. [CrossRef]
31. Oliver, W.C.; Pharr, G.M. Measurement of hardness and elastic modulus by instrumented indentation: Advances in understanding and refinements to methodology. *J. Mater. Res.* **2004**, *19*, 3. [CrossRef]
32. Uhlig, H.H. *Corrosion and Corrosion Control*; John Wiley & Sons Inc.: New York, NY, USA, 1971; p. 45.
33. Mahlobo, M.G.R.; Chikosha, L.; Olubambi, P.A. Study of the corrosion properties of powder rolled Ti–6Al–4V alloy applied in the biomedical implants. *J. Mater. Res. Technol.* **2022**, *18*, 3631–3639. [CrossRef]
34. Tokarewicz, M.; Małgorzata, G.D.; Rećko, K.; Łępicka, M.; Czajkowska, K. Investigation of the structure and corrosion resistance of novel high-entropy alloys for potential biomedical applications. *Materials* **2022**, *15*, 3938. [CrossRef]
35. Callister, W.D., Jr. *Materials Science and Engineering*; John Wiley & Sons Inc.: New York, NY, USA, 1997; p. 377.
36. Xu, Y.X.; Chen, L.; Pei, F.; Du, Y. TiAlN/CrN multilayered coatings with various modulation ratios. *Surf. Coat. Technol.* **2016**, *304*, 512–518. [CrossRef]
37. Hsu, C.H.; Lin, C.Y.; You, W.S. Microstructure and dry/wet tribological behaviors of 1% Cu-alloyed austempered ductile iron. *Materials* **2023**, *16*, 2284. [CrossRef]
38. Leyland, A.; Matthews, A. On the significance of the H/E ratio in wear control: A nanocomposite coating approach to optimised tribological behavior. *Wear* **2000**, *246*, 1–11. [CrossRef]
39. Hsu, C.H.; Lee, C.Y.; Lin, Z.H.; Ho, W.Y.; Lin, C.K. Bias effects on microstructure, mechanical properties and corrosion resistance of arc-evaporated CrTiAlN nanocomposite films on AISI 304 stainless steel. *Thin Solid Film.* **2011**, *519*, 4928–4932. [CrossRef]